NANO LETTERS

LETTER

pubs.acs.org/NanoLett

High Efficiency Dye-Sensitized Solar Cells Based on Hierarchically Structured Nanotubes

Meidan Ye,[†,‡] Xukai Xin,[†,§] Changjian Lin,[*,‡] and Zhiqun Lin[*,†,§]

[†]Department of Materials Science and Engineering, Iowa State University, Ames, Iowa 50011, United States

[‡]Department of Chemistry, College of Chemistry and Chemical Engineering, Xiamen University, Xiamen 361005, China

[§]School of Materials Science and Engineering, Georgia Institute of Technology, Atlanta, Georgia 30332, United States

Supporting Information

ABSTRACT: Dye-sensitized solar cells (DSSCs) based on hierarchically structured TiO_2 nanotubes prepared by a facile combination of two-step electrochemical anodization with a hydrothermal process exhibited remarkable performance. Vertically oriented, smooth TiO_2 nanotube arrays fabricated by a two-step anodic oxidation were subjected to hydrothermal treatment, thereby creating advantageous roughness on the TiO_2 nanotube surface (i.e., forming hierarchically structured nanotube arrays—nanoscopic tubes composed of a large number of nanoparticles on the surface) that led to an increased dye loading. Subsequently, these nanotubes were exploited to produce DSSCs in a backside illumination mode, yielding a significantly high power conversion efficiency, of 7.12%, which was further increased to 7.75% upon exposure to O_2 plasma.

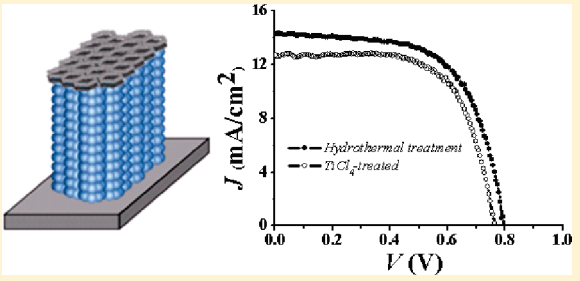

KEYWORDS: TiO_2 nanotubes, two-step anodization, hydrothermal treatment, rough surface, dye-sensitized solar cells

Dye-sensitized solar cells (DSSCs) are widely recognized as a promising alternative to conventional silicon solar cells, which usually suffer from a high cost of manufacturing and installation.[1−3] DSSCs have demonstrated power conversion efficiency, PCE, over 10% and at a very competitive cost. In these cells, the electrons generated from photoexcited dyes are injected into the conduction band of a semiconductor photoanode composed of TiO_2, while the concomitant holes are transferred through the redox electrolyte to the cathode. A great deal of research effort has been made in DSSCs to achieve improved performance, including the rational design and exploitation of a wide diversity of dyes as light absorbers,[4−7] the optimization of nanocrystalline TiO_2 photoanodes of different architectures for dye loading and electron transport,[8−11] the utilization of redox electrolytes with effective components for hole transport,[3,7,8,12] and the replacement of expensive noble metal films (e.g., platinum) with other low-cost materials to serve as back-contact electrodes.[13,14]

In DSSCs, a 10 μm thick film with a three-dimensional (3D) network composed of randomly dispersed spherical TiO_2 nanoparticles is typically employed as the photoanode.[5] However, in this disordered network the presence of numerous grain boundaries reduces electron mobility and leads to slow transport of excited electrons, thus limiting the efficiency improvement. In this context, several one-dimensional (1D) nanostructures, including nanorods, nanowires, and nanotubes, have been applied to overcome this problem.[15−17] In particular, self-organized, vertically oriented TiO_2 nanotubes provide a vectorial pathway for electron transport along the long axis of nanotubes to the collection electrode, thereby minimizing electron loss as in the case of TiO_2 nanoparticle networks due to random electron hopping across and trapping at grain boundaries.[8,18−21] Recently, TiO_2 nanotube arrays with desirable dimension and aspect ratio have been produced by electrochemical anodization of high-purity Ti foil or Ti thin films via optimization of the electrolyte temperature, applied anodization potential, and anodization time.[22−26] To date, the largest PCEs of 7.37% and 9.1% were reported on DSSCs based on TiO_2 nanotubes in backside illumination mode[27] and front side illumination mode,[28] respectively. On the other hand, for a high efficiency DSSC, large surface area is of key importance for the TiO_2 photoanode layer to maximize dye absorption and harvest adequate sunlight.[29,30] However, in comparison to sintered TiO_2 nanoparticle network films, the smooth 1D TiO_2 nanostructures often possess insufficient surface area for dye attachment.[9,31] To this end, $TiCl_4$ treatment was employed as an effective strategy to increase the surface roughness of 1D nanostructured TiO_2 and modify the cracks resulting from thermal annealing of as-prepared samples, thus improved the device performance by providing an increased surface area for dye adsorption and reducing the shunt current (i.e., increasing the shunt resistance).[6,8,27]

Herein, we report high efficiency dye-sensitized nanotube solar cells in a backside illumination mode by capitalizing on novel, hierarchically structured TiO_2 nanotubes, which were

Received: May 4, 2011
Revised: May 31, 2011
Published: July 05, 2011

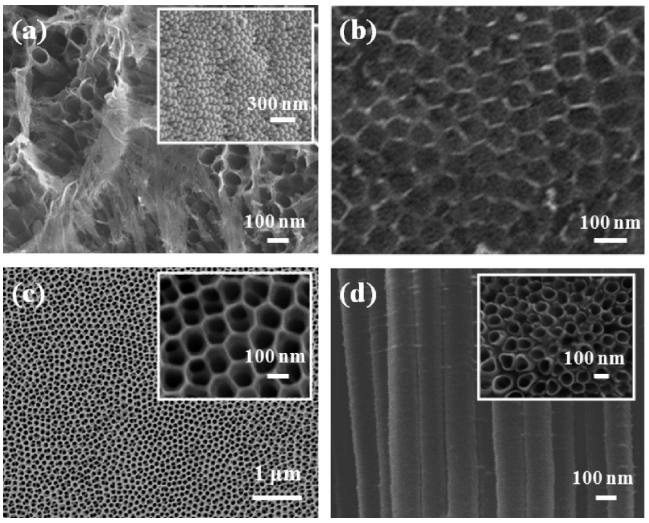

Figure 1. SEM images of TiO_2 nanotubes. (a, b) After the first anodization for 3 h: (a) top view, inset shows the bottom of nanotube; (b) the substrate after removing the nanotube layer by ultrasonication (Scheme 1c). (c, d) After the second anodization for 2 h: (c) top view of TiO_2 nanotubes covered by a mesoporous layer, inset shows magnified top view; (d) cross-sectional view, inset shows the top view of nanotubes after dissolution of the covered mesoporous layer via a lengthy anodization (i.e., 5 h).

Scheme 1. Fabrication of Hierarchically Structured TiO_2 Nanotubes via a Combination of Two-Step Anodization and Hydrothermal Treatment (or $TiCl_4$ treatment)[a]

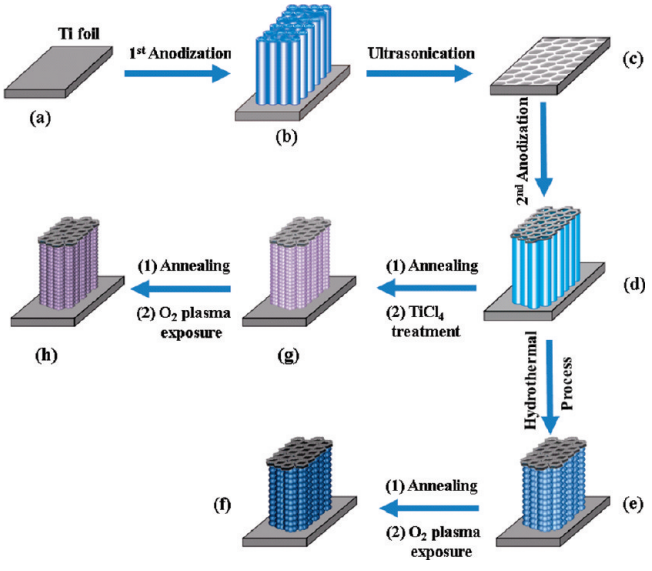

[a] The top of the TiO_2 nanotube arrays after the second anodization is covered by a layer of mesoporous TiO_2 as depicted in gray in (d–h).

rationally crafted by a combination of a two-step electrochemical anodization with hydrothermal processing. Hierarchical TiO_2 nanostructures were subsequently exploited as photoanodes and impregnated with N719 dye. In stark contrast to PCE of 4.30% for the DSSC obtained using as-prepared TiO_2 nanotube arrays under simulated AM 1.5 G irradiation of 100mW/cm^2, a markedly increased PCE of 7.12% was yielded after subsequent hydrothermal treatment (i.e., using hierarchically structured

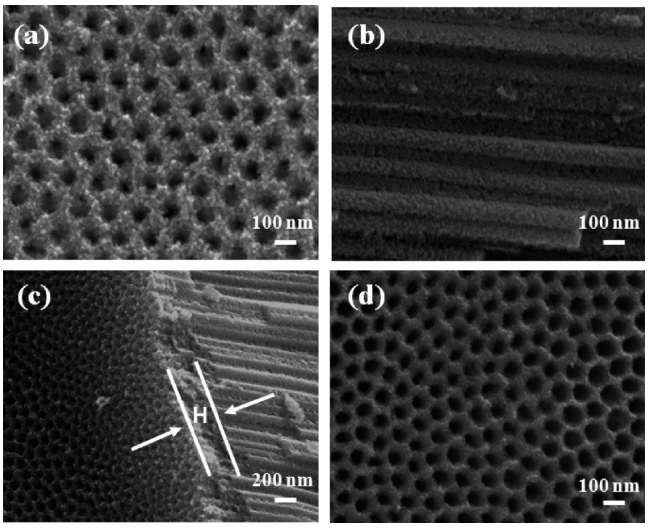

Figure 2. SEM images of two-step anodized TiO_2 nanotubes with a layer of mesoporous TiO_2 covered on the top. (a–c) After subsequent hydrothermal treatment: (a) top view; (b) cross-sectional view; (c) 3D view. *H* is the thickness of the densely packed mesoporous layer. (d) After subsequent $TiCl_4$ treatment, top view.

TiO_2 nanotubes). Notably, the PCE was further raised to 7.75% following O_2 plasma exposure. Hydrothermal processing created advantageous roughness on the surface of TiO_2 nanotubes by etching the smooth nanotube surface into a rough surface composed of small nanoparticles, thereby providing largely increased surface areas accessible to the N719 dye to maximize the N719 uptake while concurrently retaining the favorable 1D nanotubular geometry that rendered effective electron transport and electrolyte permeation.

TiO_2 nanotubes obtained after the first anodization in ethylene glycol electrolyte containing NH_4F and a small amount of water had fragile bundling debris blocking the surface as revealed by scanning electron microscopy (SEM) (Figure1a), which not only affected the electron transport but also retarded the infiltration of dye and electrolyte into nanotubes.[8,32] Thus, ultrasonication was performed to remove the debris. However, it was difficult to obtain a smooth surface, and the TiO_2 nanotube membrane was easily cracked and even delaminated during the ultrasonic treatment (Figure S1a, Supporting Information). To circumvent this problem, self-organized nanotubes without the presence of surface debris were achieved by a two-step anodization process (Scheme 1).[23,31,32] Specifically, the TiO_2 membrane formed after the first anodization was removed by ultrasonication, leaving behind a regular hexagonally packed pattern on the Ti foil surface (Scheme 1c and Figure 1b). It was then anodized again (i.e., the second anodization) to yield uniform TiO_2 nanotubes with smooth surfaces (Scheme 1d and Figure 1c). The nanotube arrays were oriented normal to the membrane surface (Figure 1d). Notably, a mesoporous layer developed on the top of the nanotubes during the second anodization that prevented the formation of thin debris and yielded vertically oriented nanotubes underneath (Scheme 1d and Figure 1c). The diameter of nanotubes after a lengthy anodization that resulted in the removal of the top mesoporous layer (inset in Figure 1d) was the same as that shown in Figure 1b, suggesting that the densely packed pattern (Scheme 1c and Figure 1b) served as a shield to guide the vertical growth of nanotubes.

dx.doi.org/10.1021/nl2014845 |*Nano Lett.* 2011, 11, 3214–3220

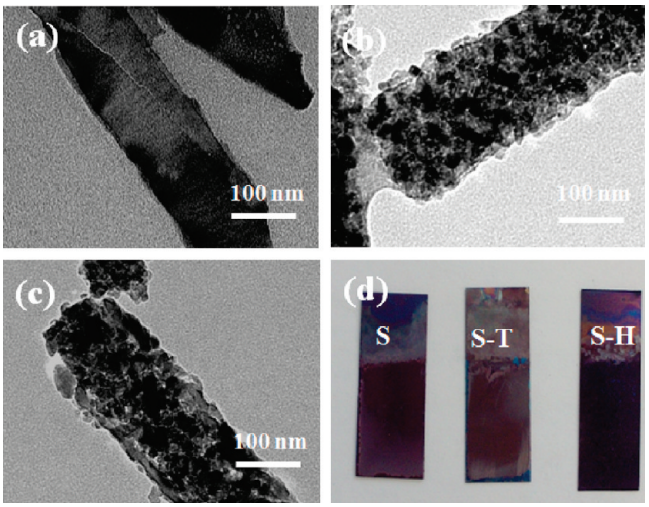

Figure 3. TEM images of two-step anodized TiO_2 nanotubes. (a) Without any posttreatment. (b) With hydrothermal treatment. (c) With $TiCl_4$ treatment. (d) Digital image of samples after N719 dye soaking. Key: S, after the second anodization without any posttreatment; S-T, after the second anodization followed by $TiCl_4$ treatment; S-H, after the second anodization followed by hydrothermal treatment.

Subsequently, nanotubes were processed by either hydrothermal treatment (Scheme 1e) or soaking in $TiCl_4$ solution (Scheme 1g). Quite intriguingly, after hydrothermal treatment the surface of smooth TiO_2 nanotubes became comparatively rough as revealed by the SEM measurement (Figure 2a). The cross-sectional SEM image showed that the nanotubular morphology was well retained and substantial nanoparticles emerged on the nanotube surface (Figure 2b), forming hierarchically structured nanotube arrays (i.e., nanoscopic tubes composed of a large number of nanoparticles on the surface). Furthermore, it is clear that the mesoporous layer formed during the second anodization (Figure 1c) still covered the top of vertically oriented nanotubes that were developed underneath (Figure 2c). It is noteworthy that the wall thickness increased from 10 nm before hydrothermal treatment (Figure 1c) to 50 nm after hydrothermal treatment (Figure 2a), and meanwhile the pore size of the top mesoporous layer decreased from 140 nm (Figure 1c) to 70 nm (Figure 2a). It is not surprising that a similar trend was observed for the sample after $TiCl_4$ treatment; the wall thickness increased to 45 nm while the pore size reduced to 80 nm (Figure 2d). It has been elucidated in literature that upon the $TiCl_4$ treatment, TiO_2 nanoparticles were produced due to the hydrolysis of Ti^{4+} (eq 1) and decorated the nanotube surface.[8] By contrast, we proposed that in the hydrothermal process, the TiO_2 nanoparticles were mainly evolved from the smooth nanotubes via a competition between two reactions, namely, hydrolysis of Ti^{4+} that favors the formation of TiO_2 nanoparticles (eq 1) and their chemical etching (i.e., dissolution) due to the presence of F^- (eqs 2 and 3).[33,34]

$$Ti^{4+} + 4H_2O \rightarrow Ti(OH)_4 + 4H^+;\quad Ti(OH)_4 \rightarrow TiO_2 + 2H_2O \tag{1}$$

$$TiO_2 + 6F^- + 4H^+ \rightarrow [TiF_6]^{2-} + 2H_2O \tag{2}$$

$$Ti^{4+} + 6F^- \rightarrow [TiF_6]^{2-} \tag{3}$$

As such, the concentration of $(NH_4)_2TiF_6$ aqueous solution, the temperature, and the duration of treatment during hydrothermal processing had to be delicately controlled to retain the integrity of the TiO_2 membrane and prevent it from completely dissolving due to overetching. Under an optimized condition the reactions occurred homogenously and high quality nanotubes composed of uniform nanoparticles on the surface can be achieved by hydrothermal processing.

Panels a–c of Figure 3 show TEM images of the corresponding TiO_2 nanotubes, in which the nanoparticles are clearly evident. Smooth nanotubes (Figure 3a) were transformed into extensively rough nanotubes via either a hydrothermal treatment with nanoparticles formed on the TiO_2 surface (Figure 3b) or a $TiCl_4$ soaking treatment with nanoparticles attached on the TiO_2 surface (Figure 3c). The physical properties of the resulting nanotubes, including the diameter and length measured by SEM or transmission electron microscopy (TEM) are summarized in Table 1 and Table S1 (Supporting Information). Hereafter, we refer to nanotubes prepared by one-step only and two-step anodizations as F nanotubes and S nanotubes, respectively. Denote F-H nanotubes and S-H nanotubes as the corresponding nanotubes after hydrothermal treatment, respectively. Regard F-T nanotubes and S-T nanotubes as the corresponding nanotubes after $TiCl_4$ treatment.

XRD measurements revealed that all TiO_2 samples were successfully converted into crystalline forms after thermal annealing at 450 °C in air (Figure 4). The emergence of (101), (200), (105), and (211) peaks suggested the formation of photoactive anatase TiO_2, while the additional peaks in the XRD profiles originated from the Ti substrate. It is important to note that there were some distinct differences in the XRD patterns. On comparison of the XRD profile of S nanotubes with S-T nanotubes (panels a and c of Figure 4), there was no observable change in the shape of peaks except for an increase in peak intensity, which can be attributed to the addition of nanoparticles on the TiO_2 nanotube surface resulting from the hydrolysis of Ti^{4+} (eq 1). In comparison to S nanotubes, the peak width of S-H nanotubes was broadened and the (200) and (211) peak intensities became relatively stronger, while the (105) peak was weakened (Figure 4a,b). Thus, the structure of TiO_2 nanotubes was changed upon hydrothermal processing. Furthermore, the average size of crystals was 10.6 nm for S-H nanotubes, calculated based on the Scherrer equation (Table S1, Supporting Information), which correlated very well with the particle size measured from SEM and TEM (Figures 2 and 3) and signified that the hydrothermally treated nanotubes were made of TiO_2 nanoparticles (eqs 2 and 3). In contrast, for S nanotubes and S-T nanotubes, the average crystal sizes were 32.6 and 29.4 nm, respectively (Table S1, Supporting Information). Compared to S nanotubes and S-T nanotubes, a 3-fold decrease in the crystal size for S-H nanotubes significantly increased the surface area, thereby leading to an increase in dye adsorption and, in turn, an improved light harvesting efficiency.[35]

All TiO_2 nanotube arrays noted above were then utilized as photoanodes to assemble dye-sensitized nanostructured solar cells, and their performances were measured (see Experimental Methods). Table 1 and Table S2 (Supporting Information) summarize the device performance of the resulting N719 dye-sensitized TiO_2 nanotube solar cells. The current–voltage (J–V) characteristics of representative samples are shown in Figure 5 and Figure S2 (Supporting Information). First, comparing F (2h)

dx.doi.org/10.1021/nl2014845 |*Nano Lett.* 2011, 11, 3214–3220

Table 1. Summary of the Performance of DSSCs Using Different TiO_2 Nanotube Arrays

sample[a]	anodization time (h)	NT length (μm)	J_{sc} (mA/cm^2)	V_{oc} (V)	FF	PCE (%)[b]
F	2.0	7.5 ± 0.4	9.18	0.66	0.63	3.79
F-H	2.0	7.6 ± 0.5	12.43	0.77	0.59	5.66
S	1.5	7.4 ± 0.4	9.12	0.70	0.62	3.98
	2.0	10.5 ± 0.4	11.74	0.72	0.51	4.30
S-H	1.0	5.8 ± 0.5	10.15	0.76	0.66	5.23
	1.5	7.5 ± 0.5	12.37	0.77	0.68	6.50
	2.0	10.6 ± 0.5	14.31	0.79	0.63	7.12
	2.5	13.4 ± 0.5	16.31	0.73	0.58	6.96
S-T	2.0	10.5 ± 0.6	12.77	0.77	0.67	6.54
S-H-O_2	2.0	10.6 ± 0.5	15.64	0.77	0.62	7.75

[a] : Nanotubes prepared under different conditions (F, first anodization; S, second anodization). F-H and S-H are corresponding TiO_2 nanotubes after hydrothermal treatment, S-T designates corresponding TiO_2 nanotubes after $TiCl_4$ treatment, S-H-O_2 designates corresponding TiO_2 nanotubes after hydrothermal treatment, followed by the O_2 plasma exposure. [b] : PCE (%) = J_{sc} V_{oc} FF/P_{in}, where P_{in} = 100 mW/cm^2.

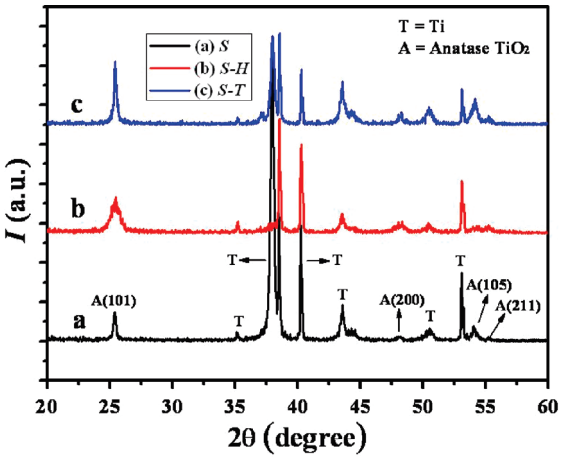

Figure 4. XRD patterns of TiO_2 nanotube arrays prepared under different conditions after thermal annealing: (a) S, without any post-treatment; (b) S-H, after hydrothermal treatment; (c) S-T, after $TiCl_4$ treatment.

nanotubes with S (2h) nanotubes prepared with the same anodization time (i.e., 2 h), solar cells assembled using S (2h) nanotubes with a length of 10.5 μm exhibited a higher PCE of 4.30% than a PCE of 3.79% for F (2h) nanotubes with a length of 7.5 μm (Figure 5a and Table1). This was due primarily to greater dye loading for longer nanotubes, indicating a faster growth rate of nanotubes in the second anodization. We note that the solar cells fabricated by using S (1.5h) nanotubes with a length of 7.4 μm showed a relatively higher PCE of 3.98% (Table 1) than that of F (2h) nanotubes of comparable length; this may be ascribed to the presence of a clean and smooth surface in the S nanotube sample as discussed above, thus promoting dye absorption. A similar trend was seen for samples that were posttreated with a hydrothermal procedure for which the performance of F−H (2h) nanotubes (PCE = 5.66%, Figure 5a and Table 1) was lower that of S−H (1.5h) nanotubes (PCE = 6.50%, Figure 5b and Table 1). This was attributed to the presence of aggregates on the nanotube surface in the former sample (panels b and c of Figure S1, Supporting Information), which originated from the surface debris after the first anodization; their presence hindered dye and electrolyte diffusion into the nanotubes.

Second, a markedly enhanced device performance was witnessed via the use of hydrothermally treated nanotubes. As the length of nanotubes was increased, the PCE increased and the highest performance was achieved from the sample anodized for 2 h with a length of 10.6 μm, exhibiting an open circuit voltage, V_{oc} of 0.79 V, a short circuit current, J_{sc} of 14.31 mA/cm^2, a fill factor, FF, of 0.63, and a PCE of 7.12% (i.e., S-H (2h) sample in Figure 5b and Table 1); this represented a 65% increase in PCE as compared to the S (2h) sample (i.e., PCE of 4.30% in Figure 5a and Table 1). Notably, with the use of ever longer TiO_2 nanotube arrays (i.e., the S−H (2.5h) sample with a tube length of 13.4 μm), the reduction in V_{oc} of 0.73 V and FF of 0.58 offset the increase in J_{sc} of 16.31 mA/cm^2, thereby resulting in a decreased PCE of 6.96% (Figure 5b and Table 1). Thus, the S-H (2h) sample was chosen to conduct the O_2 plasma exposure study as discussed below.

Third, $TiCl_4$ treatment has been widely used to improve the DSSC efficiency;[18] thus solar cells using $TiCl_4$-treated TiO_2 nanotubes were also prepared and their performances were evaluated and compared with those of hydrothermally treated samples as noted above. As shown in Figure 5c, a PCE of 6.54% was obtained for an S-T (2h) sample prepared with the same anodization time (i.e., 2 h). It can be concluded that a higher J_{sc} (i.e., J_{sc} = 14.31 mA/cm^2 by hydrothermal processing vs J_{sc} = 12.77 mA/cm^2 by $TiCl_4$ treatment in Table 1) and higher V_{oc} (i.e., V_{oc} = 0.79 V by hydrothermal processing $_{vs}$ $^{V_{oc}}$ = 0.77 V by $TiCl_4$ treatment) contributed to a higher performance for the hydrothermally treated sample (i.e., PCE = 7.12%). Similar trends were observed for solar cells assembled using F-T (2h; *PCE* = 5.13%), S-T (1h; PCE = 4.06%), and S-T (1.5h; PCE = 5.61%) TiO_2 nanotube arrays; that is, the PCEs of solar cells with $TiCl_4$ treatment were lower than those that were hydrothermally treated (i.e., F-H: 2h, PCE = 5.66%. S-H: 1h, PCE = 5.23%. S-H: 1.5h, PCE = 6.50%) by comparing the values in Table S2 (Supporting Information) and Table 1.

Finally, to further improve the efficiency of dye-sensitized nanostructured solar cells, samples were exposed to O_2 plasma prior to the adsorption of N719 dye (Scheme 1f and h). We have previously shown that upon O_2 plasma exposure, the number of hydroxyl groups on the TiO_2 surface increased and eventually saturated; this increased the N719 dye loading capacity by forming interfacial bonding between N719 and the TiO_2 via the coupling reaction of terminal carboxylic acid groups on N719 with complementary hydroxyl groups on the TiO_2 surface,

dx.doi.org/10.1021/nl2014845 |*Nano Lett.* 2011, 11, 3214–3220

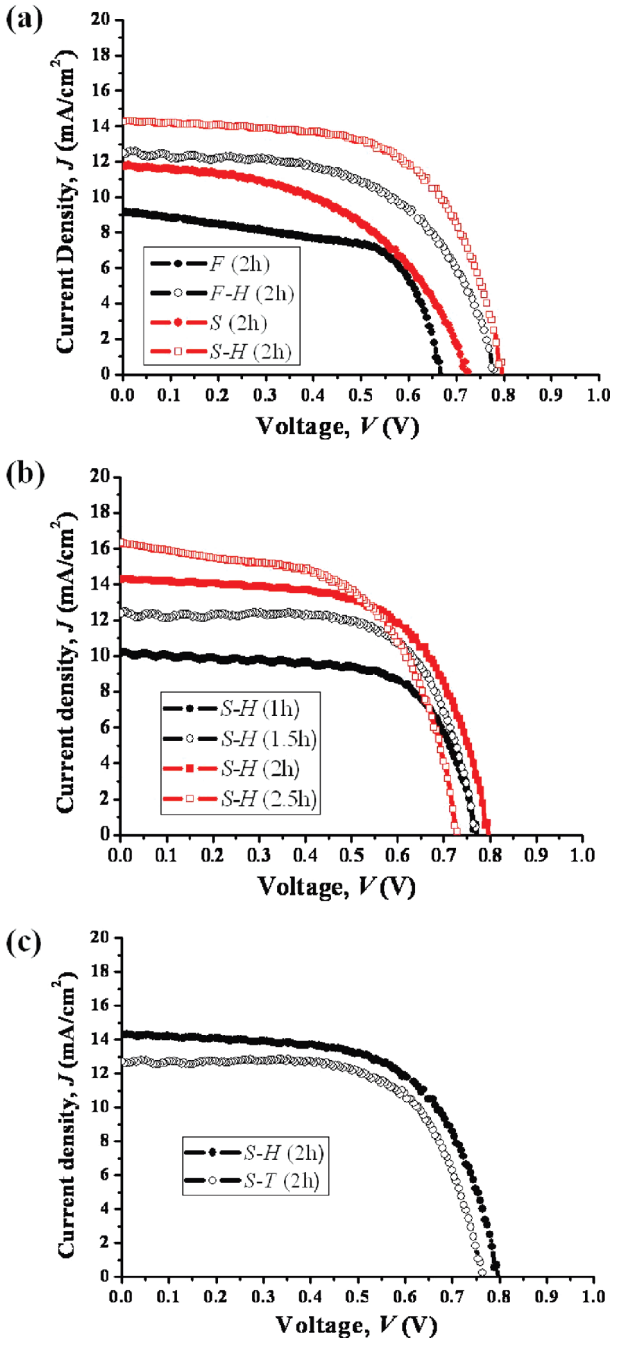

Figure 5. $J-V$ characteristics of DSSCs using TiO_2 nanotube arrays. (a) Nanotubes fabricated by only one-step anodization (black solid circles), only one-step anodization followed by hydrothermal treatment (black open circles), two-step anodization (red solid circles), two-step anodization followed by hydrothermal treatment (red open squares); anodization time = 2 h. (b) Nanotubes fabricated by two-step anodization at different anodization times (i.e., 1, 1.5, 2, and 2.5 h), followed by hydrothermal treatment. (c) Nanotubes fabricated by two-step anodization, followed by either hydrothermal (solid circles) or $TiCl_4$ (open circles) treatment.

thereby substantially regulating the interfacial charge transfer from N-719 dye to TiO_2 and, therefore, the ultimate photophysical properties at the nanoscale.[27] In the present study the optimum condition of a 10 min O_2 plasma exposure was applied according to our previous work.[27] A PCE of 7.75% was yielded for the S-H-O_2 (2h) sample, reflecting an 8.8% increase in the efficiency compared to the S-H (2h) sample without O_2 plasma treatment (i.e., PCE = 7.12%) (Table 1 and Figure S2, Supporting Information). Similarly, improvements were also observed for other O_2 plasma treated nanotubes (i.e, S-O_2 (2h), PCE = 4.66% and S-T-O_2 (2h), PCE = 6.72%, respectively) (Table S2 and Figure S2, Supporting Information).

For DSSCs, the capacity of dye loading exerts a profound influence on the photocurrent density. To this end, the amount of adsorbed N719 dyes was estimated by measuring the eluted dye molecules from nanotubes with UV−vis absorption spectroscopy. It is worth noting that the dye concentrations were 4.7×10^{-8} mol/cm^2 for S nanotubes, 5.2×10^{-8} mol/cm^2 for S-T nanotubes, and 7.5×10^{-8} mol/cm^2 for S-H nanotubes, respectively (Table S1, Supporting Information). The results suggested that the S-T nanotube sample had 1.11 times higher dye adsorption than the S nanotube sample, while it was 1.60 times for the S-H nanotube sample. When compared with the S-T nanotube sample, the S-T nanotube sample possessed 1.44 times higher dye adsorption. Moreover, the digital image in Figure 3d shows that the S-H nanotube sample displayed a darker color than the S nanotube sample and S-T nanotube sample after soaking in the N719 dye solution, which was indicative of the improved dye loading of S-H nanotubes, consistent with the results measured by UV−vis spectroscopy. As the enhanced dye loading was a direct consequence of the increased surface area of TiO_2 nanotube arrays, it can be concluded that the improved performance for photovoltaic devices produced by employing S-H nanotubes was strongly correlated with the rough surface created by hydrothermal processing of nanotubes and, correspondingly, largely alleviated the disadvantage of increased grain boundaries between small nanoparticles formed during the hydrothermal treatment.

In summary, we have developed hierarchically structured TiO_2 nanotubes composed of nanoparticles with reduced crystal size by capitalizing on hydrothermal processing, thereby yielding more surface area for dye anchoring. The nanotubes were then exploited as the photoanode to produce DSSCs in a backside illumination mode, exhibiting a high PCE of 7.12%, which was further raised to 7.75% upon subsequent O_2 plasma treatment. In addition to ruthenium-based organic dyes, in principle, conjugated homopolymers, all conjugated block copolymers, and semiconductor nanocrystals can be utilized as alternative photosensitizers to create a wide range of DSSCs based on hydrothermally treated TiO_2 nanotubes. Hydrothermal processing may stand out as a simple and promising modification route to impart rough surfaces on one-dimensional large band gap semiconductors for use in DSSCs with markedly enhanced performance.

Experimental Methods. *Fabrication of Hierarchically Structured TiO_2 Nanotube Arrays.* Highly ordered TiO_2 nanotube arrays were fabricated by electrochemically anodizing Ti foils (2.5 cm × 1.0 cm in size, 250 μm thick, 99.7% purity; Sigma-Aldrich) in a two-electrode electrochemical cell.[24] Briefly, all anodizations were carried out by using Ti foil as a working electrode and platinum foil as a counter electrode at room temperature. All Ti foils were degreased with acetone and ethanol for about 15 min by ultrasonication, respectively, then rinsed with distilled water, and finally dried in air prior to use. The cleaned Ti foil was first anodized in a 200 mL ethylene glycol solution containing 0.3 wt % NH_4F and 2 vol % H_2O (i.e., 4 mL of H_2O and 196 mL of ethylene glycol) at 50 V for 3 h

dx.doi.org/10.1021/nl2014845 |*Nano Lett.* 2011, 11, 3214–3220

(Scheme 1b). The resulting nanotube film was then removed by ultrasonication for a few seconds, leaving behind hexagon-like footprints on the Ti foil surface (Scheme 1c). A second anodization was then performed under the same condition for 2 h to produce well-aligned TiO_2 nanotubes in which a layer of mesopores was formed on the top (Scheme 1d). Subsequently, the two-step anodized nanotubes were transferred to a Teflon-lined autoclave containing 15 mL of 0.01 M $(NH_4)_2TiF_6$ aqueous solution, and heated at 115−120 °C for 15−20 min (Scheme 1e), followed by annealing at 450 °C for 2 h in air to transform amorphous TiO_2 into crystalline photoactive anatase form. TiO_2 nanotubes fabricated by only one-step anodization (i.e., only the first anodization for 2 h) were also prepared for comparison. As for other comparisons, $TiCl_4$ treatment was also performed by immersing preannealed TiO_2 nanotubes in 100 mL of 0.2 M $TiCl_4$ aqueous solution in a 70 °C oil bath for 30 min (Scheme 1g), followed by annealing in air at 450 °C for 30 min. In order to improve the device performance, prior to dye adsorption, samples fabricated by a two-step anodization followed by either hydrothermal treatment or $TiCl_4$ treatment were further exposed to O_2 plasma at 30 W power for 10 min (Scheme 1, f and h, respectively).[27]

TiO_2 Nanotube Solar Cells Fabrication. To fabricate DSSCs, all TiO_2 nanotubes described above were soaked in anhydrous ethanol containing 0.2 mM commercially available N719 dyes (*cis*-diisothiocyanato-bis(2,2′-bipyridyl-4,4′-dicarboxylato) ruthenium(II) bis(tetrabutylammonium); Solaronix Co.) and kept for 24 h at room temperature. Platinum (Pt) counter electrodes were prepared by dropping 0.5 mM H_2PtCl_6 isopropanol solution on FTO glass, followed by heating at 400 °C for 20 min. Dye-sensitized TiO_2 nanotube arrays with an active area of approximately 0.12 cm^2 were assembled together with the Pt-coated FTO glass by applying a 25 μm thick hot-melt sealed film as the spacer (SX1170-25; Solaronix Co.). The redox electrolyte used in the study was an ionic liquid containing 0.60 M BMIM-I, 0.03 M I_2, 0.50 M TBP, and 0.10 M GTC in a mixture of acetonitrile and valeronitrile (v/v = 85/15) (No. ES-0004, purchased from io.li.tec, Germany). The electrolyte was injected between two electrodes and driven by capillary force through the hole on the hot-melt sealed film. As the Ti foil was not transparent, light had to enter the cell through the Pt-coated FTO glass, yielding dye-sensitized hierarchically structured TiO_2 nanotube solar cells in a *backside illumination mode*.[19,27]

Characterization. The morphology and microstructure of nanotubes were examined by field emission scanning electron microscopy (FE-SEM; FEI Quanta 250, operated at 20 kV under high vacuum) and transmission electron microscopy (TEM, JEOL 2100, operated at 200 kV). Phase identification of TiO_2 was conducted by X-ray diffraction (XRD; SCINTAG XDS-2000, Cu Kα radiation). The current−voltage ($J-V$) characteristics were measured using a Keithley model 2400 multisource meter. A solar simulator (SoLux Solar Simulator) was used to simulate sunlight for an illumination intensity of 100 mW/cm^2 as calibrated with a Daystar Meter.

■ ASSOCIATED CONTENT

Ⓢ Supporting Information. SEM images of TiO_2 nanotubes prepared by one-step anodization, performances of DSSCs using different TiO_2 nanotubes, and $J-V$ characteristics of DSSCs using TiO_2 nanotube arrays treated by O_2 plasma exposure. This material is available free of charge via the Internet at http://pubs.acs.org.

■ AUTHOR INFORMATION

Corresponding Author

*E-mail: cjlin@xmu.edu.cn and zhiqun.lin@mse.gatech.edu.

■ ACKNOWLEDGMENT

M.Y. gratefully acknowledges the financial support from the Chinese Scholarship Council. C.L. gratefully acknowledges the financial support from the National Natural Science Foundation of China (51072170, 21021002) and the National High Technology Research and Development Program of China (2009AA03Z327).

■ REFERENCES

(1) Oregan, B.; Gratzel, M. *Nature* **1991**, *353*, 737–740.
(2) Gratzel, M. *Nature* **2001**, *414*, 338–344.
(3) Nakade, S.; Kanzaki, T.; Wada, Y.; Yanagida, S. *Langmuir* **2005**, *21*, 10803–10807.
(4) De Angelis, F.; Fantacci, S.; Selloni, A.; Gratzel, M.; Nazeeruddin, M. K. *Nano Lett.* **2007**, *7*, 3189–3195.
(5) Gao, F.; Wang, Y.; Shi, D.; Zhang, J.; Wang, M. K.; Jing, X. Y.; Humphry-Baker, R.; Wang, P.; Zakeeruddin, S. M.; Gratzel, M. *J. Am. Chem. Soc.* **2008**, *130*, 10720–10728.
(6) Shankar, K.; Bandara, J.; Paulose, M.; Wietasch, H.; Varghese, O. K.; Mor, G. K.; LaTempa, T. J.; Thelakkat, M.; Grimes, C. A. *Nano Lett.* **2008**, *8*, 1654–1659.
(7) Shi, D.; Cao, Y. M.; Pootrakulchote, N.; Yi, Z. H.; Xu, M. F.; Zakeeruddin, S. M.; Graetzel, M.; Wang, P. *J. Phys. Chem. C* **2008**, *112*, 17478–17485.
(8) Chen, C. C.; Chung, H. W.; Chen, C. H.; Lu, H. P.; Lan, C. M.; Chen, S. F.; Luo, L.; Hung, C. S.; Diau, E. W. G. *J. Phys. Chem. C* **2008**, *112*, 19151–19157.
(9) Chou, T. P.; Zhang, Q. F.; Russo, B.; Fryxell, G. E.; Cao, G. Z. *J. Phys. Chem. C* **2007**, *111*, 6296–6302.
(10) Wu, J. J.; Chen, G. R.; Lu, C. C.; Wu, W. T.; Chen, J. S. *Nanotechnology* **2008**, *19*, 105702.
(11) Chen, D. H.; Huang, F. Z.; Cheng, Y. B.; Caruso, R. A. *Adv. Mater.* **2009**, *21*, 2206.
(12) Yanagida, S.; Yu, Y. H.; Manseki, K. *Acc. Chem. Res.* **2009**, *42*, 1827–1838.
(13) Hong, W. J.; Xu, Y. X.; Lu, G. W.; Li, C.; Shi, G. Q. *Electrochem. Commun.* **2008**, *10*, 1555–1558.
(14) Ramasamy, E.; Chun, J.; Lee, J. *Carbon* **2010**, *48*, 4563–4565.
(15) Cheng, H. M.; Chiu, W. H.; Lee, C. H.; Tsai, S. Y.; Hsieh, W. F. *J. Phys. Chem. C* **2008**, *112*, 16359–16364.
(16) Liu, B.; Aydil, E. S. *J. Am. Chem. Soc.* **2009**, *131*, 3985–3990.
(17) Gonzalez-Valls, I.; Lira-Cantu, M. *Energy Environ. Sci.* **2009**, *2*, 19–34.
(18) Mor, G. K.; Shankar, K.; Paulose, M.; Varghese, O. K.; Grimes, C. A. *Nano Lett.* **2006**, *6*, 215–218.
(19) Paulose, M.; Shankar, K.; Varghese, O. K.; Mor, G. K.; Hardin, B.; Grimes, C. A. *Nanotechnology* **2006**, *17*, 1446–1448.
(20) Zhu, K.; Neale, N. R.; Miedaner, A.; Frank, A. J. *Nano Lett.* **2007**, *7*, 69–74.
(21) Roy, P.; Kim, D.; Lee, K.; Spiecker, E.; Schmuki, P. *Nanoscale* **2010**, *2*, 45–59.
(22) Wang, J.; Lin, Z. Q. *J. Phys. Chem. C* **2009**, *113*, 4026–4030.
(23) Wang, J.; Zhao, L.; Lin, V. S. Y.; Lin, Z. Q. *J. Mater. Chem.* **2009**, *19*, 3682–3687.
(24) Wang, J.; Lin, Z. Q. *Chem. Mater.* **2008**, *20*, 1257–1261.
(25) Yoriya, S.; Grimes, C. A. *Langmuir* **2010**, *26*, 417–420.

(26) Kang, S. H.; Kim, H. S.; Kim, J. Y.; Sung, Y. E. *Nanotechnology* **2009**, *20*, 355307.
(27) Wang, J.; Lin, Z. Q. *Chem. Mater.* **2010**, *22*, 579–584.
(28) Lin, C. J.; Yu, W. Y.; Chien, S. H. *J. Mater. Chem.* **2010**, *20*, 1073–1077.
(29) Sauvage, F.; Chen, D. H.; Comte, P.; Huang, F. Z.; Heiniger, L. P.; Cheng, Y. B.; Caruso, R. A.; Graetzel, M. *ACS Nano* **2010**, *4*, 4420–4425.
(30) Shao, W.; Gu, F.; Li, C. Z.; Lu, M. K. *Ind. Eng. Chem. Res.* **2010**, *49*, 9111–9116.
(31) Ghadiri, E.; Taghavinia, N.; Zakeeruddin, S. M.; Gratzel, M.; Moser, J. E. *Nano Lett.* **2010**, *10*, 1632–1638.
(32) Roy, P.; Albu, S. P.; Schmuki, P. *Electrochem. Commun.* **2010**, *12*, 949–951.
(33) Li, S. Q.; Zhang, G. M.; Guo, D. Z.; Yu, L. G.; Zhang, W. *J. Phys. Chem. C* **2009**, *113*, 12759–12765.
(34) Wang, D. A.; Yu, B.; Wang, C. W.; Zhou, F.; Liu, W. M. *Adv. Mater.* **2009**, *21*, 1964–1967.
(35) Park, K. H.; Gu, H. B.; Jin, E. M.; Dhayal, M. *Electrochim. Acta* **2010**, *55*, 5499–5505.